

**REPORT DOCUMENTATION PAGE**

*Form Approved  
OMB No. 0704-0188*

The public reporting burden for this collection of information is estimated to average 1 hour per response, including the time for reviewing instructions, searching existing data sources, gathering and maintaining the data needed, and completing and reviewing the collection of information. Send comments regarding this burden estimate or any other aspect of this collection of information, including suggestions for reducing the burden, to Department of Defense, Washington Headquarters Services, Directorate for Information Operations and Reports (0704-0188), 1215 Jefferson Davis Highway, Suite 1204, Arlington, VA 22202-4302. Respondents should be aware that notwithstanding any other provision of law, no person shall be subject to any penalty for failing to comply with a collection of information if it does not display a currently valid OMB control number.

**PLEASE DO NOT RETURN YOUR FORM TO THE ABOVE ADDRESS.**

<b>1. REPORT DATE (DD-MM-YYYY)</b> 30-11-2011		<b>2. REPORT TYPE</b> Final Performance Report		<b>3. DATES COVERED (From - To)</b> From 01-05-2006 To 30-11-2011	
<b>4. TITLE AND SUBTITLE</b> (MURI FY06) INFRARED AND TERAHERTZ LASERS ON SI USING NOVEL GROUP-IV ALLOYS				<b>5a. CONTRACT NUMBER</b>	
				<b>5b. GRANT NUMBER</b> FA9550-06-1-0442	
				<b>5c. PROGRAM ELEMENT NUMBER</b>	
				<b>5d. PROJECT NUMBER</b>	
				<b>5e. TASK NUMBER</b>	
<b>6. AUTHOR(S)</b> J. Menéndez (Arizona State University) J. Kouvetakis (Arizona State University) A.V.G. Chizmeshya (Arizona State University) S.-L. Chuang (University of Illinois at Urbana) G. Sun (University of Massachusetts Boston)				<b>5f. WORK UNIT NUMBER</b>	
<b>7. PERFORMING ORGANIZATION NAME(S) AND ADDRESS(ES)</b> Arizona State University at the Downtown Phoenix campus 411 N. Central Avenue, Phoenix, AZ 85004 Phone: 602-496-INFO (4636)				<b>8. PERFORMING ORGANIZATION REPORT NUMBER</b>	
<b>9. SPONSORING/MONITORING AGENCY NAME(S) AND ADDRESS(ES)</b> AFOSR / RSE 875 North Randolph Street, Suit 325 Room 3112 Arlington, Virginia 22203-1768				<b>10. SPONSOR/MONITOR'S ACRONYM(S)</b> AFOSR / RSE	
				<b>11. SPONSOR/MONITOR'S REPORT NUMBER(S)</b> AFRL-OSR-VA-TR-2012-0161	
<b>12. DISTRIBUTION/AVAILABILITY STATEMENT</b> 1) DISTRIBUTION STATEMENT A: Approved for public release; distribution is unlimited					
<b>13. SUPPLEMENTARY NOTES</b>					
<b>14. ABSTRACT</b> This project started on May 1, 2006 and ended November 30, 2011 after a final 6-month no-cost extension. The total 5-year budget was \$2,500,000. The main goal of the project was to advance the materials science of Sn-based semiconductor alloys for use in laser structures monolithically integrated on Si platforms. As of December 2011, a total of 49 publications acknowledge support from this grant, 1-49 and 9 patents have been awarded for inventions generated by the program participants in the field of new group-IV semiconductors.					
<b>15. SUBJECT TERMS</b> Standard terms apply					
<b>16. SECURITY CLASSIFICATION OF:</b>			<b>17. LIMITATION OF ABSTRACT</b>	<b>18. NUMBER OF PAGES</b>	<b>19a. NAME OF RESPONSIBLE PERSON</b>
<b>a. REPORT</b>	<b>b. ABSTRACT</b>	<b>c. THIS PAGE</b>			Gernot S. Pomrenke, RSE (Program Manager)
U	U	U	UU		<b>19b. TELEPHONE NUMBER (Include area code)</b> 703.696.8426

Reset

**Award FA9550-06-1-0442**

**(MURI FY06) INFRARED AND TERAHERTZ LASERS ON SI  
USING NOVEL GROUP-IV ALLOYS**

**PIs:**

**J. Menéndez (Arizona State University)  
J. Kouvetakis (Arizona State University)  
A.V.G. Chizmeshya (Arizona State University)  
S.-L. Chuang (University of Illinois at Urbana)  
G. Sun (University of Massachusetts Boston)**

**Final Report**

## Summary

This project started on May 1, 2006 and ended November 30, 2011 after a final 6-month no-cost extension. The total 5-year budget was \$2,500,000. The main goal of the project was to advance the materials science of Sn-based semiconductor alloys for use in laser structures monolithically integrated on Si platforms. As of December 2011, a total of 51 publications acknowledge support from this grant,<sup>1-51</sup> and 9 patents have been awarded for inventions generated by the program participants in the field of new group-IV semiconductors.

## Ge/GeSn/GeSiSn materials on Si

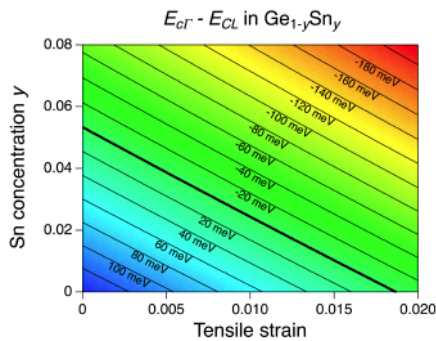


**Figure 1** Energy separation between the conduction band minima at the  $\Gamma$  and  $L$  points of the Brillouin zone in the Ge-like band structure of GeSn alloys. The tensile strain is biaxial in the (001) plane. The thick line indicates the direct-indirect cross-over.

These activities focused on improving the GeSn and GeSiSn materials that were key to the program and on the determination of their physical and optical properties. The value of GeSn for Si-based optoelectronics is based on the fact that the addition of Sn reduces the band gap, shifting absorption to near-IR spectral ranges of great interest, and at the same times reduces the separation between the direct and indirect conduction band minima, making the material potentially more valuable than pure Ge for laser applications. This is summarized in Fig. 1. Ternary GeSiSn alloys, on the other hand, offer much more versatile electronic and lattice properties due to the two degrees of compositional freedom, which should allow for the independent tuning of the optical properties and lattice constant. This is schematically illustrated in Fig. 2. Due to this versatility, GeSiSn alloys were viewed as a key component of several device ideas, including lasers and solar cells.

At the start of the program in 2006, only GeSn alloys had been grown directly on Si substrates, whereas GeSiSn alloys required GeSn-buffered Si substrates and custom precursors. In addition, only  $n$ -type doping of GeSn alloys had been demonstrated. The fine-tuning of the growth protocols for GeSn alloys on Si, described in Ref. 30, made it possible to attain excellent control of composition and achieve superb crystallinity, as evidenced by x-ray and RBS channeling experiments. The availability of high-quality alloy samples over a broad compositional range enabled detailed studies of the compositional dependence of the lattice parameter<sup>45</sup> the thermal expansivity,<sup>58</sup> and the Raman phonon frequencies.<sup>1,10</sup>

The ternary GeSiSn alloys, introduced by Bauer *et al.* in 2003,( Ref. 52) were initially grown on GeSn-buffered Si using the non-commercial CVD precursor  $\text{SiH}_3\text{GeH}_3$ . Shortly before the start of the MURI program, the precursor portfolio for the growth of GeSiSn on GeSn-buffered Si was extended to  $(\text{GeH}_3)_2\text{SiH}_2$  and  $(\text{GeH}_3)_3\text{SiH}$ .<sup>53</sup> These materials were improved with MURI support. In addition, the growth of

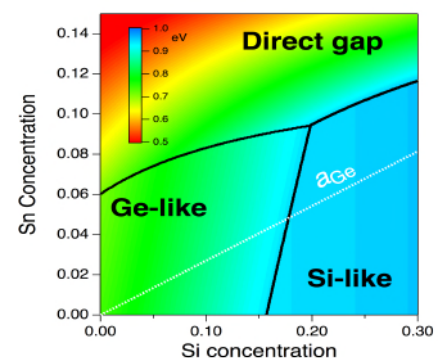


**Figure 2** Electronic structure “phase diagram” for GeSiSn alloys. The white line shows the compositions for which the lattice constant matches that of pure Ge.

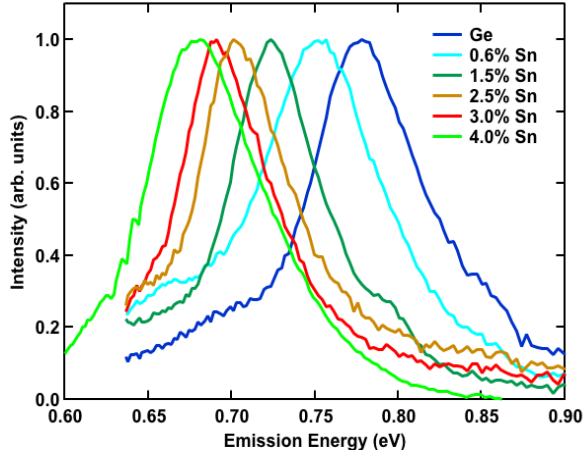


**Figure 3** Normalized, room temperature PL spectra of intrinsic  $\text{Ge}_{1-y}\text{Sn}_y$  with  $y \sim 0.0 - 0.04$  showing the direct gap peak ( $E_0$ ) and low energy shoulder corresponding to the indirect gap.

$\text{GeSiSn}$  using the commercial precursors  $\text{Si}_3\text{H}_8$ ,  $\text{Ge}_2\text{H}_6$ , and  $\text{SnD}_4$  was demonstrated,<sup>17</sup> and a method was discovered to grow  $\text{GeSiSn}$  alloys directly on (001) Si substrates without intermediate buffer layers.<sup>31,42</sup> More recently, the synthetic approach used to develop  $\text{GeSn}$  alloys was extended to the limit of ultra-small Sn concentrations, leading to high-quality layers on Si which for all practical purposes behave as pure Ge films.<sup>46</sup>

Dramatic progress in the development of doping protocols of  $\text{GeSn}$  and  $\text{GeSiSn}$  alloys was achieved under the MURI program. Acceptor doping of  $\text{GeSn}$  alloys was reported in 2009.<sup>21,28</sup> Both  $n$ -type and  $p$ -type doping of  $\text{GeSiSn}$  was reported the same year.<sup>24</sup> These breakthroughs paved the way for the development of device structures, described below.

## Optical properties of $\text{GeSn}$ and $\text{GeSiSn}$ semiconductors

Spectroscopic ellipsometry was the main technique used for the initial studies of the optical properties of  $\text{GeSn}$  and  $\text{GeSiSn}$  alloys. Systematic studies of the compositional dependence of the main optical transitions in  $\text{GeSn}$  preceded the MURI program, and led to the discovery of scaling relationships in the bowing parameters for group-IV alloys.<sup>54,55</sup> Under the MURI program detailed measurements of the optical constants were reported, with the idea of generating useful databases for device designs.<sup>30</sup> Important progress in the understanding of the near band gap absorption were developed with the introduction of models that accurately reproduce the experimental data when excitonic effects are taken into account.<sup>30</sup>

A review article on the properties of ternary  $\text{SiGeSn}$  alloys<sup>33</sup> included information on band gap compositional dependencies, deformation potential interpolation schemes, and expressions for the dependence of important band edges as a function of composition and strain. Measurements on this system demonstrated for the first time decoupling of band structure and strain in a group-IV alloy.<sup>23</sup>

The second phase of optical studies started with the observation of photoluminescence (PL) from  $\text{GeSn}$  alloys (Fig. 3).<sup>37</sup> This breakthrough required a systematic post-growth optimization, including rapid thermal annealing and annealing under  $\text{H}_2$  exposure. The observation of PL in intrinsic films was followed by the study of optical emission in doped  $n$ -type films.<sup>47,48</sup> This work led to insights into the origin of the photoluminescence in Ge-like materials grown

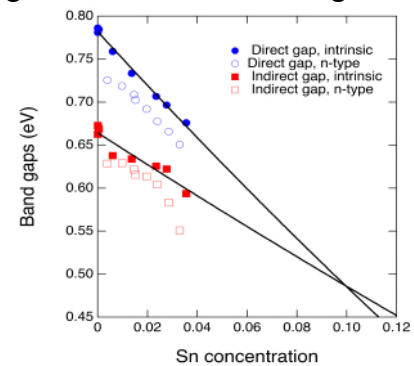


**Figure 4** Direct and indirect band gaps in  $\text{GeSn}$  alloys extracted from PL data. The solid symbols represent intrinsic alloys, whereas the empty symbols correspond to  $n$ -type samples with concentrations in the  $10^{19} \text{ cm}^{-3}$  range. The energy shift of the two band edges in the doped samples is due to band gap renormalization.

on Si substrates. The detailed and systematic studies of the PL signal of doped and undoped films made it possible to extract the compositional dependence of both the direct and indirect edges, as shown in Fig. 4. This work suggests that the direct-indirect crossover occurs for Sn concentrations close to 10%, in agreement with our own theoretical predictions from 2006.<sup>54</sup>

## Device fabrication and testing

Devices based on GeSn and GeSiSn alloys had to be developed literally “from scratch”, starting with the introduction of doping strategies, as described above, and the development of suitable fabrication protocols, including metallization. The first devices reported were simple photoconductor structures whose main objective was to advance our etching, oxidation, and metallization recipes.<sup>18</sup> This was followed by the introduction of the first GeSn heterostructure *pin* diodes,<sup>29</sup> which have been systematically improved since their introduction.<sup>56,57</sup> Considerable financial and personnel investments were made to establish facilities for the testing of these devices, since our group’s background was originally in materials science. The I-V characteristics of the fabricated diodes are excellent. A comparison with data in the literature can only be made for GeSn devices in the limit of vanishing Sn concentrations, and in this case our fabricated diodes have dark currents systematically below those reported for comparable devices of similar responsivity. This implies extremely low dislocation densities, as suggested in Fig. 6.

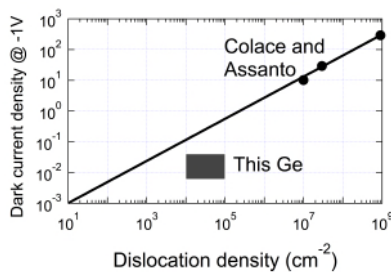


**Figure 6** Empirical dark current vs dislocation density relationship for Ge-on-Si heterostructure diodes, as determined by Colace and Assanto. The dots represent data from other groups. The shaded rectangle indicates the dislocation energy range and dark current range for samples grown at ASU.

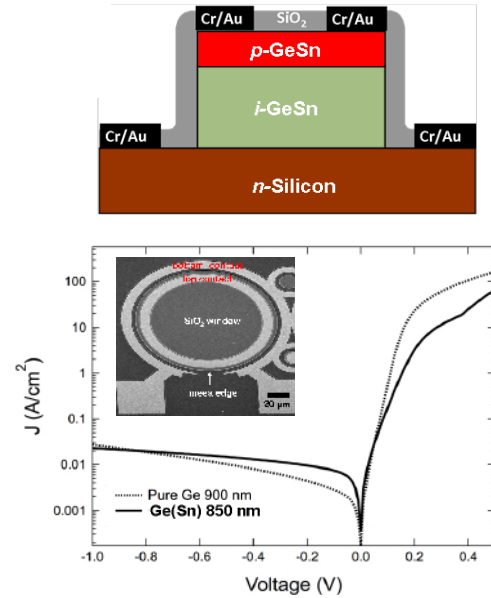


**Figure 5** The top panel shows a schematic diagram of the fabricated diodes. The lower panel shows typical IV curves, and the inset shows a top view of a selected device.

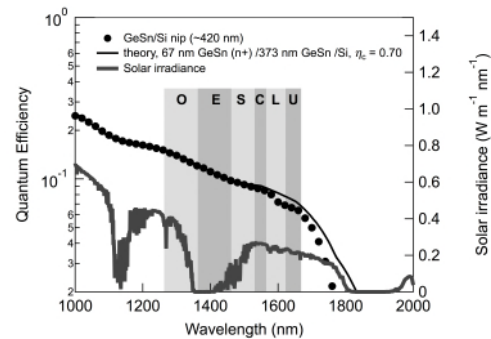


**Figure 7** External quantum efficiency of a GeSn/Si heterostructure *pin* diode. The solid line is a theoretical calculation assuming a collection efficiency of 70%. The vertical bars correspond to the different telecom windows. The bottom curve shows the solar irradiance spectrum in the same wavelength range, suggesting possible photovoltaic applications for these devices.

Responsivity studies of the fabricated diodes (Fig. 7) display the main characteristic expected from GeSn alloys, namely the shift of the absorption onset towards longer wavelengths. This is of great technological significance, since the incorporation of Sn dramatically enhances the responsivity at 1.55  $\mu\text{m}$  and extends the useful range of the diode to the entire range of telecom bands. Moreover, Sn concentrations as small as 2% are capable of capturing a significant fraction of the near-IR solar spectrum for which pure Ge is transparent, suggesting possible applications in next-generation multi-junction solar cells. Finally, a fundamental breakthrough on our way to a laser device was achieved with the observation of electroluminescence from GeSn *pin* diodes (Fig. 8).<sup>58</sup>

Work is still underway to demonstrate lasing in simple optically pumped laser structures as seen in Fig. 9. Evidence of gain in some structures has already been obtained, and we expect demonstrate lasing shortly. These initial structures have low Sn concentrations and are not expected to be direct gap materials, but quasi-direct conditions can be achieved by heavily *n*-type doping.

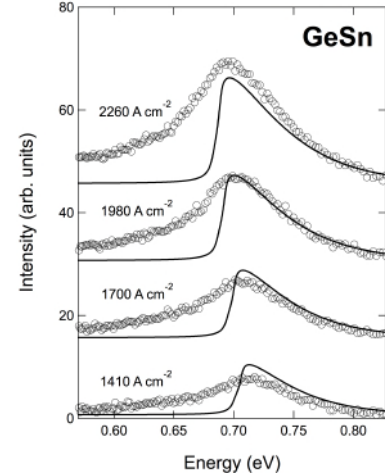


**Figure 8** Electroluminescence spectra from a GeSn/Si heterostructure *pin* diode at different injection currents. The solid lines are theoretical fits.

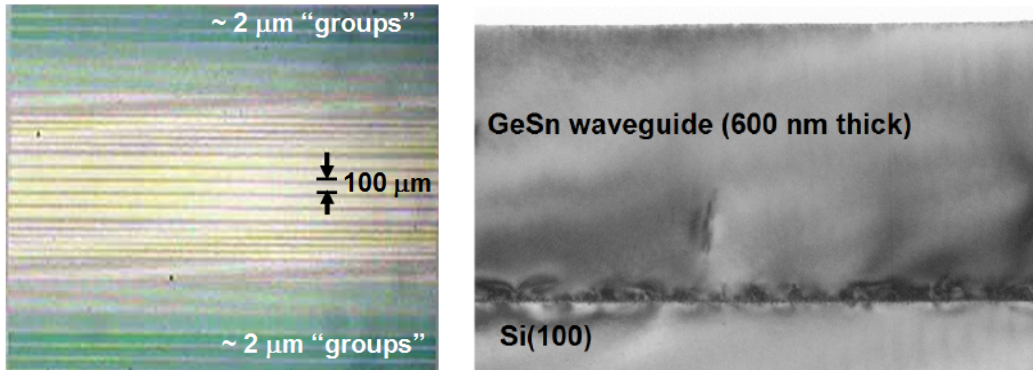


**Figure 9** (left) Optical image of GeSn waveguides fabricated as rectangular slabs with dimensions of 4 mm in length, 1.6-100 microns in width and 430-620  $\mu\text{m}$  in height. The green bands at bottom and top of the image correspond to ensembles of parallel 1.6 micron wide devices. The lighter features in the middle represent single 100 micron wide devices. (right) XTEM micrograph of a single waveguide showing that the structure remains essentially defect-free post device processing.

## Device design and simulation

### University of Illinois (Chuang)

A complete design of the  $\text{Ge}_{1-z}\text{Sn}_z\text{-Ge}_x\text{Si}_y\text{Sn}_{(1-x-y)}$  strain-balanced multi-quantum well (MQW) laser structure was proposed by Chuang's group at the University of Illinois.<sup>5,25</sup> The introduction of compressive strain into the  $\text{Ge}_{1-z}\text{Sn}_z$  layers modifies the valence band structure to reduce the threshold carrier density. In addition, the calculation shows that the compressive strain makes the

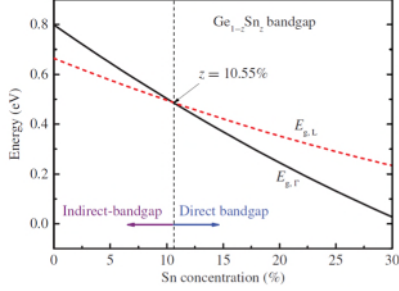


**Figure 10** Direct and indirect band gaps of the unstrained  $\text{Ge}_{1-z}\text{Sn}_z$  alloys as a function of  $\alpha$ -Sn concentration.

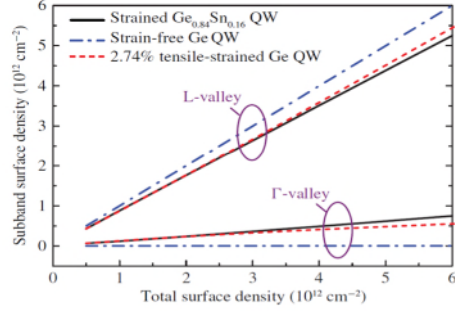


**Figure 11** The surface carrier densities in the L-valley and the  $\Gamma$ -valley for different quantum well structures Ref. 50.

band gap closer to a direct band gap and, thus, a better chance for lasing action is expected. The direct and indirect band gaps as a function of the  $\alpha$ -Sn concentration is shown in Fig. 10. With the increase of the  $\alpha$ -Sn concentration, the direct and indirect band gaps decrease but the direct gap reduces faster due to the negative band gap of  $\alpha$ -Sn. When the Sn concentration is larger than 10.55%, the direct band gap is smaller than the indirect band gap and, thus, laser action is expected to be achievable. In the  $\text{Ge}_{1-z}\text{Sn}_z$  system, however, due to a large density of state of the  $L$  conduction band and its similar energy band gap to  $\Gamma$  conduction band, most of the injected carrier density will fall into the  $L$  conduction band. With a good strain design, the rest of injected carrier density into the  $\Gamma$  conduction band can be sufficient to lead to lasing action. Fig. 11 shows the carrier densities in the  $L$ -valley and  $\Gamma$ -valley for different quantum wells. Clearly, when compressive strain  $\text{Ge}_{1-z}\text{Sn}_z$  and tensile strain Ge are introduced, the band gap of the quantum well is equal or smaller than that of the  $L$  conduction band, and, thus the carrier density in the  $\Gamma$  conduction band is increased. Fig. 12 shows the material gain of the TE mode for the  $\text{Ge}_{0.84}\text{Sn}_{0.16}$  quantum well as a function of the carrier density with the consideration of the  $L$  conduction band minima. The gain from the TE mode is dominant since the compressive strain lifts up the heavy hole valence band. The  $2,500 \text{ cm}^{-1}$  of peak gain at  $2,883 \text{ nm}$  is comparable with those of many conventional III-V semiconductor lasers.

On the other hand, a waveguide design was also presented as depicted in Fig. 13. Since the  $p$ - and  $n$ - contact layers have slightly smaller refractive indices than that of the quantum wells, the optical field will spread out from the waveguide due to the small refractive index contrast,

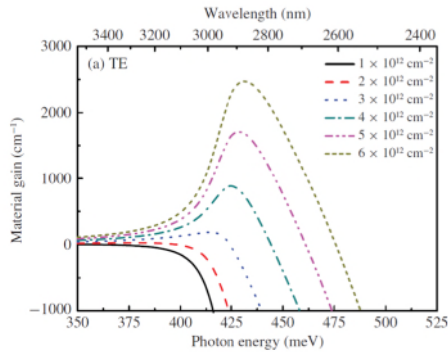


**Figure 12** The material gain of the TE mode as a function of the injected surface carrier density. The peak gain is located at around  $2,800 \text{ nm}$ . Ref. 50.

especially at such a long wavelength. By employing silica on the ridge waveguide, the high index contrast can be provided. The confinement factor can reach 6.98%.<sup>51</sup> With the consideration of the free-carrier absorption in the  $n$ -doped buffer layer and the  $p$ -contact layer, the threshold modal gain is around  $100 \text{ cm}^{-1}$  for a  $500\text{-}\mu\text{m}$  long cavity and  $2\text{-}\mu\text{m}$  wide waveguide, which corresponds to a threshold carrier density of  $4.364 \times 10^{18} \text{ cm}^{-3}$  and is equivalent to a current density of  $9.78 \text{ kA/cm}^2$ . The results show the feasibility of realizing  $\text{Ge}_{1-z}\text{Sn}_z\text{-Ge}_x\text{Si}_y\text{Sn}_{(1-x-y)}$  QW lasers. The introduction of tensile strain Ge quantum well is also

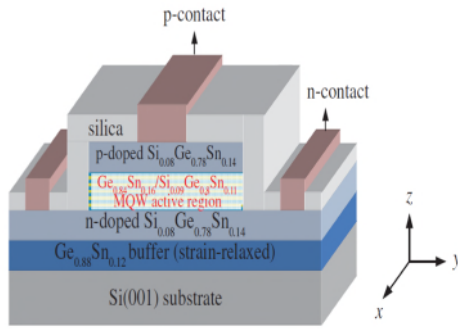


**Figure 12.** Our proposed laser-structure design based on a strain-balanced GeSn/GeSiSn MQW system .Ref. 50.

proposed and the details can be found in Ref. 25. We believe that our analysis in this project provides a clear guidance for future design for  $\text{Ge}_{1-z}\text{Sn}_z\text{-Ge}_x\text{Si}_y\text{Sn}_{(1-x-y)}$  and  $\text{Ge-Ge}_x\text{Si}_y\text{Sn}_{(1-x-y)}$  quantum-well lasers.

## University of Massachusetts Boston

### Quantum Cascade Laser design

The Group at UMass Boston performed the design and simulation using three different approaches based on group-IV elements (Si, Ge, Sn) and their alloys. One approach employs the scheme of intersubband transitions (IST) in lattice matched  $\text{Ge}/\text{Ge}_{1-x-y}\text{Si}_x\text{Sn}_y$  heterostructure to develop a strain-free quantum cascade laser (QCL) that operates in the  $L$ -valley.<sup>4</sup> The other approaches are based on band-to-band transitions in lattice matched GeSn/GeSiSn where type-I confined direct-bandgap active region is formed with the use of either a double heterostructure

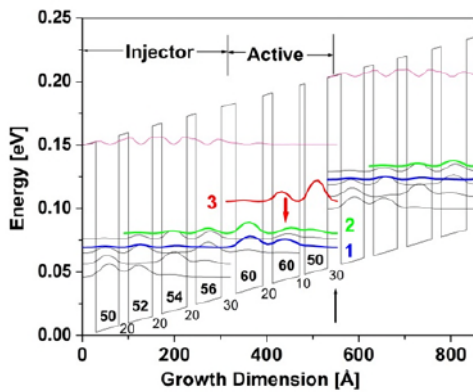


**Figure 13** L-valley conduction band profile and squared envelope functions under an electric field of 10kV/cm. Layer thicknesses in angstrom are marked with bold numbers for Ge QWs and regular for GeSiSn barriers

(DH)(Ref. 43) or a multiple quantum well (MQW) structure.<sup>44</sup>

Lasers based on IST in SiGe quantum wells (QWs) could circumvent the issue of band gap indirectness. Electroluminescence has been observed from Si-rich Si/SiGe quantum cascade structures, but lasing has eluded researchers. One common difficulty in these efforts is the use of holes instead of electrons for IST because most of the band offset between the Si-rich SiGe QWs and the Si barriers is in the valence band. Incorporation of Sn provides the opportunity to engineer separately the strain and band structure in  $\text{Ge}_{1-x-y}\text{Si}_x\text{Sn}_y$  since we can vary the Si ( $x$ ) and Sn ( $y$ ) compositions independently. It can be shown that a conduction-band offset of 150 meV at  $L$ -valleys can be obtained between lattice-matched Ge and  $\text{Ge}_{0.76}\text{Si}_{0.19}\text{Sn}_{0.05}$  alloy while all other conduction-band valleys ( $\Gamma$ ,  $X$ ) are above the  $L$ -valley band edge of the  $\text{Ge}_{0.76}\text{Si}_{0.19}\text{Sn}_{0.05}$  barrier. This band alignment presents a desirable alloy composition from which a QCL operating at  $L$ -valleys can be designed using Ge as QWs and

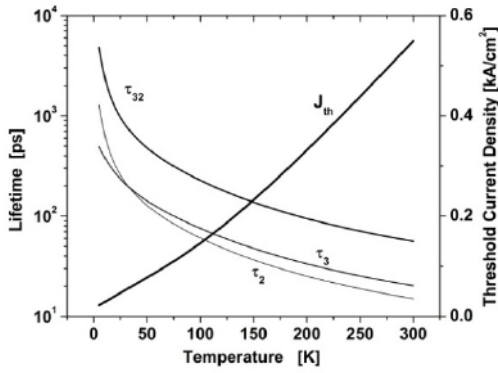


**Figure 14** Lifetimes and threshold current density as a function of operating temperature.

range of 5K to 300K. The threshold current density  $J_{th}$  is determined for a TM-polarized mode in a QCL structure of 40 periods that is confined by double-Au-plasmon waveguide with near unity optical confinement and waveguide loss 110/cm, and an assumed mirror loss of 10/cm for a typical cavity length of 1mm.  $J_{th}$  ranges from 22A/cm<sup>2</sup> at 5K to 550A/cm<sup>2</sup> at 300K as shown in Fig. 14. Since all QCL layers are lattice matched to Ge, a Ge buffer layer on a Si substrate is necessary for the entire structure to be deposited strain-free on Si substrate.

### Double Heterostructure Lasers

It is feasible to choose the compositions of GeSn and SiGeSn in such a way that they not only form type-I band alignment but also are lattice matched. Such a structure is ideal for the design of a simple DH laser. The analysis of carrier lifetime in the lattice matched Ge<sub>0.94</sub>Sn<sub>0.06</sub>/Ge<sub>0.75</sub>Si<sub>0.15</sub>Sn<sub>0.1</sub> DH reveals that at higher temperatures, the Auger process is more dominant than the radiative recombination (Fig. 15). Optical gain is calculated (Fig. 16) as a

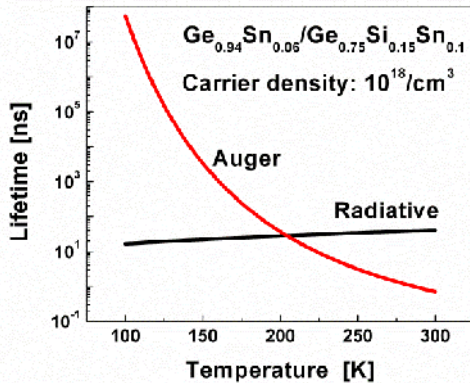


**Figure 15** Radiative and Auger recombination lifetime for a carrier concentration of 10<sup>18</sup> cm<sup>-3</sup> in the DH laser

Ge<sub>0.76</sub>Si<sub>0.19</sub>Sn<sub>0.05</sub> as barriers without the complexity arising from other energy valleys.

Fig.13 shows the QCL structure based upon Ge/Ge<sub>0.76</sub>Si<sub>0.19</sub>Sn<sub>0.05</sub> QWs. Only *L*-valley conduction-band lineups are shown in the potential diagram under an applied electric field of 10 kV/cm. The lasing transition at the wavelength of 49 μm is between the upper laser state 3 and the lower laser state 2. The result on simulation of this QCL is shown in Fig. 14 for the subband lifetimes and threshold current density for the temperature range of 5K to 300K. These lifetimes are at least one-order of magnitude longer than those of III-V QCLs owing to the nonpolar nature of GeSiSn alloys. The necessary condition for population inversion  $\tau_{32} > \tau_2$  is satisfied throughout the temperature

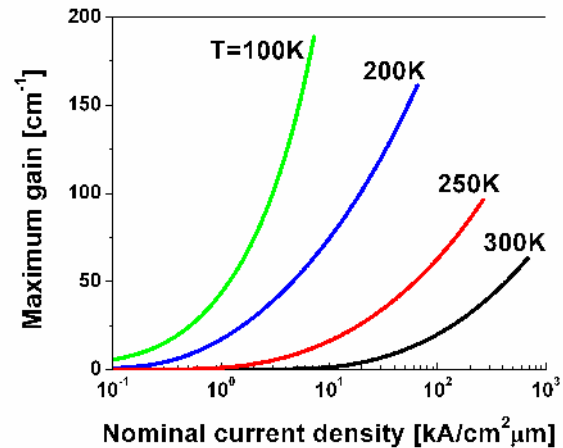


**Figure 16** Maximum optical gain as a function of the nominal current density for the temperature range from 100K to 300K.

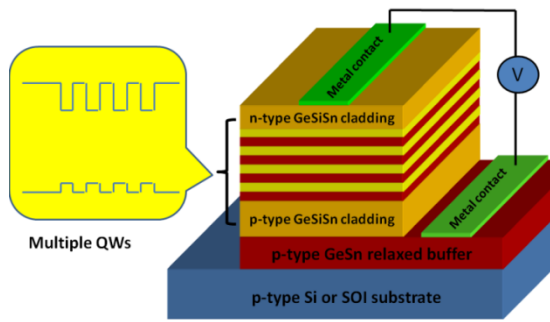


**Figure 17** GeSn/GeSiSn QW laser device on a lattice matched GeSn relaxed buffer on Si.

function of the nominal current density for a temperature range from 100K to 300K. The nominal current density can be converted to current density by multiplying the thickness of the active layer, i.e. the region of  $\text{Ge}_{0.94}\text{Sn}_{0.06}$ . At  $T=300\text{K}$ , for an active region of  $0.1\mu\text{m}$ , the current density that is required to compensate for loss of  $20\text{cm}^{-1}$  exceeds  $10\text{KA}/\text{cm}^2$ , and needs to be much higher if more loss exists. Such a large pumping current makes room temperature lasing rather unlikely in the  $\text{Ge}_{0.94}\text{Sn}_{0.06}/\text{Ge}_{0.75}\text{Si}_{0.15}\text{Sn}_{0.1}$  DH. Picking a reasonable “ceiling” for current density, it can be concluded that the GeSn DH laser requires cryogenic cooling in the 100 to 200 K range.

### Multiple Quantum Well Lasers

In order to develop group-IV band-to-band lasers that can operate at room temperature, lattice matched  $\text{Ge}_{0.9}\text{Sn}_{0.1}/\text{Ge}_{0.75}\text{Si}_{0.1}\text{Sn}_{0.15}$  MQWs as the active region has been designed as shown in

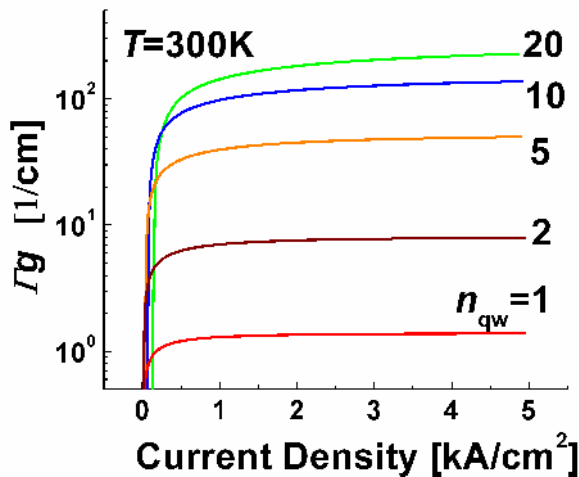


**Figure 18** Modal gain as a function of the injection current density at 300 K for the  $\text{Ge}_{0.9}\text{Sn}_{0.1}/\text{Ge}_{0.75}\text{Si}_{0.1}\text{Sn}_{0.15}$  QW laser with different number of QWs.

Fig. 17. The lower density of states in the MQWs suppresses the Auger recombination, which leads to the situation where the carrier lifetime is dominated by the radiative recombination process.

Taking into account the mode confinement, we have evaluated the model gain. The result at the lasing photon energy of  $0.541\text{eV}$  ( $\lambda = 2.3\mu\text{m}$ ) as a function the injection current density is shown in Fig. 18 at 300K for the  $\text{Ge}_{0.9}\text{Sn}_{0.1}/\text{Ge}_{0.75}\text{Si}_{0.1}\text{Sn}_{0.15}$  QW laser with different numbers of QWs, but all of the lasers have 20nm QWs and 20nm barriers. Figure 18 shows that an adequate number of QWs must be designed to overcome a certain level of losses. Simulation has shown that the proposed MQW laser is suitable for room temperature operation.

### Quantum Simulations

The MURI team at ASU (Chizmeshya) routinely used quantum-based simulations, at both the molecular and solid-state levels, as a complementary tool in developing a detailed understanding of the synthesis of new materials and their properties throughout the course of the project. Solid state simulations using state-of-the-art density functional theory methodologies, implemented on

supercomputers, have enabled our group to fully elucidate the structural, optical, vibrational, thermoelastic and thermodynamic behavior of group IV systems being investigated experimentally. Our efforts in this regard focused on the influence of atomic level distribution on the optical band gap in ternaries lattice matched to Ge – an effect that is difficult to establish experimentally. For SiGeSn systems containing significant concentrations of Sn, discrete quasi-random structural models were used to investigate the role of Sn nanoclusters on various properties of Si-Ge-Sn systems (e.g., thermoelastic, thermodynamic, optical).<sup>31,35</sup> Our earlier work on  $\text{Si}_{1-x}\text{Sn}_x$  alloys, which represent the “SiSn” component of the SiGeSn ternary, suggested that nanoscale tuning of the Sn distribution within the alloy can have a profound effect on the value of the band gap for a given Sn content. The electronic band energies of the random SiGeSn alloys are calculated following a full structural optimization which yields composition-dependent cell parameters in excellent agreement with the corresponding experimental structural parameters. As shown in the representative plots in Figure 19 for an alloy with composition  $\text{Ge}_{0.45}\text{Si}_{0.44}\text{Sn}_{0.11}$  (lattice matched to Ge), simulations indicate a systematic increase in the band gap with Si and Sn concentration up a maximum value of  $\sim 1.1$  eV, followed by a small decrease for larger concentrations of Si/Sn, in semi-quantitative agreement with the experiment. However, as can be seen in part (b) of the figure nano-clustering of Sn tends to reduce the band gap by 50% over random alloys which typically containing only  $\sim 1.6\%$  Sn-Sn bonds. More significantly the simulations indicate the possibility that clustering of Sn can alter the character

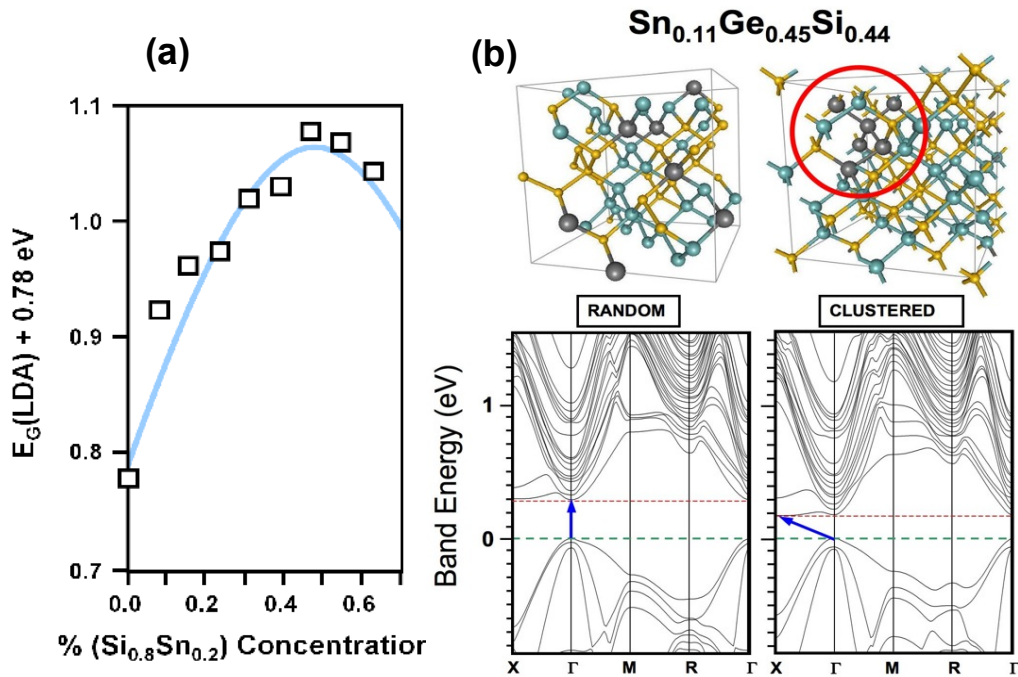


**Figure 19** (a) LDA band gap dependence on  $\%(\text{Si}_{0.8}\text{Sn}_{0.2})$  indicating a gradual increase of the gap to a maximum value of 1.08 eV for  $\text{Si}_{0.44}\text{Ge}_{0.45}\text{Sn}_{0.11}$ . (b) LDA electronic band structure in the vicinity of the band gap for a  $\text{Si}_{0.44}\text{Ge}_{0.45}\text{Sn}_{0.11}$  alloy with Si/Sn ratio of 4, in which the Sn atoms are randomly distributed (left), or clustered (right). In this example the Sn clustering reduces the gap by 50% and alters the character of the transition from  $G \rightarrow G$  to  $G \rightarrow X$  (note: the  $k$ -space points refer to a simple cubic supercell, not the traditional FCC primitive cell). Legend: Silicon (yellow), Germanium (blue), Tin (grey).

of the band gap from direct to indirect.

It is interesting to note that alloys with 5-8% Sn content (SiGe-like regime) are observed to exhibit facile formation and a remarkable thermal stability in spite of their high Sn content. In our recent MURI supported simulation studies we used first principles based thermodynamics to explain the origin of stability in these systems.<sup>31</sup> The main conclusion from our simulation work is that the SiGeSn ternaries are significantly more stable than their binary SnGe counterparts *with the same Sn content*. As shown in Fig. 20, at 400 °C the GeSn and SiGeSn alloys are predicted to become metastable for Sn contents above 2% and 12% respectively, in good agreement with experimental observation. Our models suggest that the presence of three elements increases the mixing entropy contribution for the ternary relative to that of the binary, thereby leading to an increased stability for the same Sn content.

### Molecular Simulations

The development of compounds with the functionalities and optical properties needed for the MURI project begun with the rational design of new enabling chemical sources for the targeted synthesis of solids. In the case of the novel photonic Si-Ge-Sn alloys, first principles molecular simulations played a crucial role in establishing the identity (via spectroscopy) and stability (via thermodynamic analysis) of a range of specialized precursors, including: (1) hydrides directly incorporating Si-Sn and Ge-Sn bonds,<sup>32</sup> (2) CMOS compatible chlorinated hydrides containing Si-Ge bonds<sup>3,13</sup> low temperature selective group applications (3) novel methyl hydride sources for the deposition of thick and high-purity Ge-rich materials<sup>6</sup> and (4) specialized hydrides containing cores with III-(IV)<sub>3</sub> composition, such as P(SiH<sub>3</sub>)<sub>3</sub>, for use as low-temperature dopant atom delivery sources in the growth of activated (doped and superdoped) Si-Ge-Sn alloys.<sup>21,26</sup>

## Novel materials

As a byproduct of the intense synthetic effort, several families of materials of potential interest for a variety of applications were introduced. This section summarizes these advances.

### Novel tunable Si<sub>3</sub>N<sub>4</sub>-like dielectric alloys containing phosphorous

One of the byproducts of the molecular synthesis efforts is the occasional discovery of alternative (value-added) applications for the newly developed precursors. Such is the case for the P(SiH<sub>3</sub>)<sub>3</sub> dopant delivery agents, which provide a straightforward and flexible synthetic basis for producing a range of new Si-P-N materials, based on their reactions with NH<sub>3</sub>. As illustrated in Figure 1, controlled mixtures of P(SiH<sub>3</sub>)<sub>3</sub> (and in some cases appropriate additions of N(SiH<sub>3</sub>)<sub>3</sub>) produce air-stable and thermally robust Si<sub>3</sub>(P<sub>x</sub>N<sub>1-x</sub>)<sub>4</sub> solids which incorporate P and N atoms in a trigonal bonding configurations reminiscent of the classic Si<sub>3</sub>N<sub>4</sub> alpha or beta structures. Here molecular and solid-state quantum simulations again played a pivotal role in

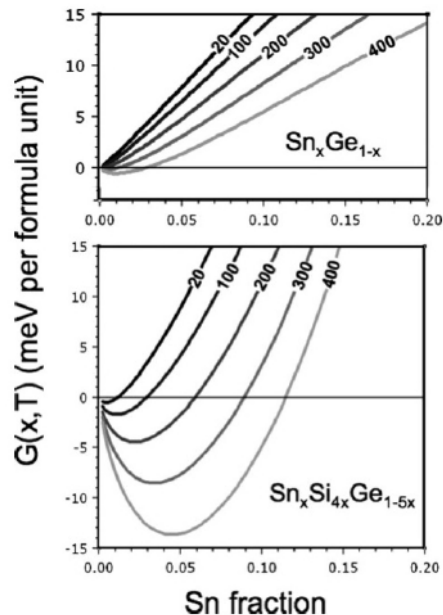


**Figure 20** Compositional dependent Gibbs free energies for binary and ternary group-IV alloys.

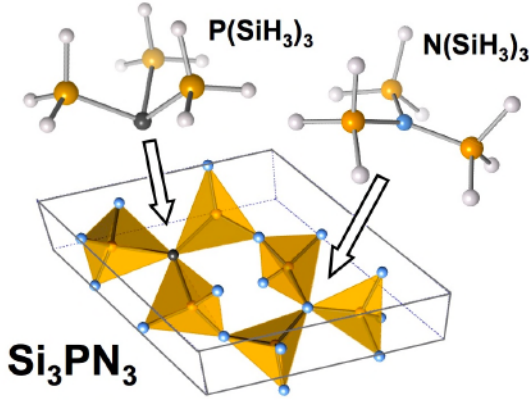


**Figure 21** Proposed structure of the newly introduced  $\text{Si}_3\text{PN}_3$  compound.

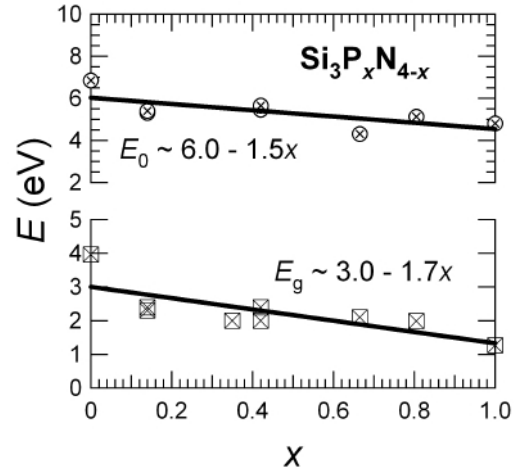


**Figure 22** Compositional dependence of the  $E_0$  and  $E_g$  band gaps in the Tauc-Lorentz model for  $\text{Si}_3\text{N}_{4-x}\text{P}_x$ .

elucidating the composition-structure relationship, including the prediction of decreasing optical band gap with increasing P content. This was confirmed by our ellipsometric measurements, as shown in Fig 22.<sup>40</sup> These materials, which represent a synergetic experiment/theory effort, may represent a new unique class of chemically compatible alternatives to silicon dioxide ( $\text{SiO}_2$ ) and silicon nitride ( $\text{Si}_3\text{N}_4$ ), the traditional dielectric and passivation materials in semiconductor devices.

Er-doped  $\text{Si}_3\text{N}_4$  has attracted attention as a possible route to the development of Si-compatible lasers at 1.55  $\mu\text{m}$ . It has been found that an excess amount of Si (so-called silicon rich nitrides – SRN) lowers the band gap of the matrix and enhances its absorption coefficient, leading to higher Er excitation cross sections.<sup>59</sup> Unfortunately, excess Si also shortens the Er emission lifetime, which reduces the Er emission efficiency.<sup>59</sup> It thus appears that this technological approach would benefit from the ability to lower the band gap of the matrix independently of the Si concentration as can be accomplished with our  $\text{Si}_3\text{N}_{4-x}\text{P}_x$  alloys .

### Si-Ge based oxynitrides

We briefly explored the formation of new Si-Ge based oxynitride materials, again from the perspective of tunable dielectric properties in a chemically compatible context. We note that materials based on compositions Si-Ge-O-N continue to attract considerable attention as functional components in a variety of high-technology applications in the areas of microelectronic and optoelectronic, including telecommunication. The “nano-synthesis” approach adopted in this study is based on reactions of disiloxane in a large excess of ammonia, where the molecular Si-O-Si cores of  $(\text{SiH}_3)_2\text{O}$  deliver both the compositional and bonding configuration at the nanoscale required to form the desired solid-state material, as illustrated in Fig. 23. Extensive computational/simulation studies were undertaken to elucidate the related formation reactions and compare the thermochemistry involved in the formation of  $\text{Si}_{1-x}\text{Ge}_x\text{N}_2\text{O}$  oxynitrides based on reactions of both  $(\text{SiH}_3)_2\text{O}$  and  $(\text{GeH}_3)_2\text{O}$  molecules, and a proposed (hypothetical)  $\text{SiH}_3\text{OGeH}_3$  analogue, in an ambient of ammonia.<sup>41</sup> From an experimental perspective, the recent development of industrial scale synthesis for  $(\text{SiH}_3)_2\text{O}$  suggests that Ge-

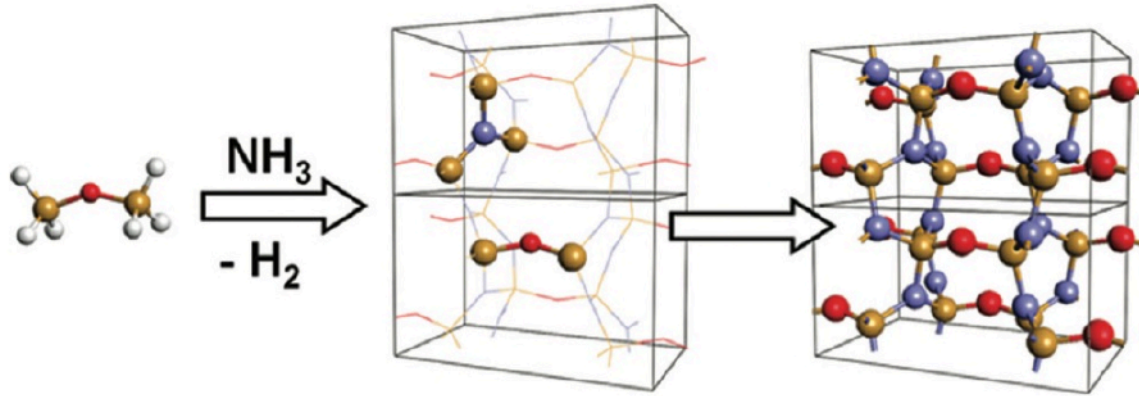


**Figure 23** “Nano-synthesis” concept as a schematic, showing the assembly of -Si-O-Si- molecular cores (left) to form the Si<sub>2</sub>N<sub>2</sub>O (right). The central panel highlights the coordination of the oxygen and nitrogen atoms with respect to the silicon sublattice nearest neighbors.

based analogues proposed in our study might be accessed using similar approaches, opening the door to novel and immediately useful Si-Ge-O-N high-k gate materials for high mobility Si-Ge based applications.

### Novel (III-V)-IV alloys

Most recently, a dramatic breakthrough was achieved with the introduction of an entirely new approach to the growth of (III-V)-IV alloys. Alloys of Group-IV and III-V semiconductors exhibit a fascinating interplay between the zincblende symmetry, which requires that the group III and group V elements be located on separate sublattices, and the diamond structure, where the two sublattices are equivalent.<sup>60-65</sup> A few material systems have been investigated so far, ranging from BNC<sub>2</sub> (a hybrid between diamond C and c-BN),<sup>66</sup> to (Ge<sub>2</sub>)<sub>1-x</sub>(GaSb)<sub>x</sub> (Ref. 67). A (III-V)-(IV) alloy subclass of particular interest are materials whose Group-IV and III-V components have very similar lattice constants (Si/AlP, Ge/GaAs/AlAs, Sn/InSb). Since the band gaps of these parent compounds are different, the corresponding alloys are good candidates for applications that require a tunable band at a fixed lattice constant. For example, a (Ge<sub>2</sub>)<sub>1-x</sub>(GaAs)<sub>x</sub> alloy, with  $x$  adjusted to obtain a band gap close to 1 eV, has been identified as candidate to be incorporated as a fourth junction in Ge/InGaAs/InGaP 3-junction solar cells.<sup>63</sup> Unfortunately, severe phase separation effects have historically hindered these potentially exciting applications as well as the systematic exploration of the very rich physics of (III-V)-(IV) alloys.<sup>63</sup> Because of these issues the interest

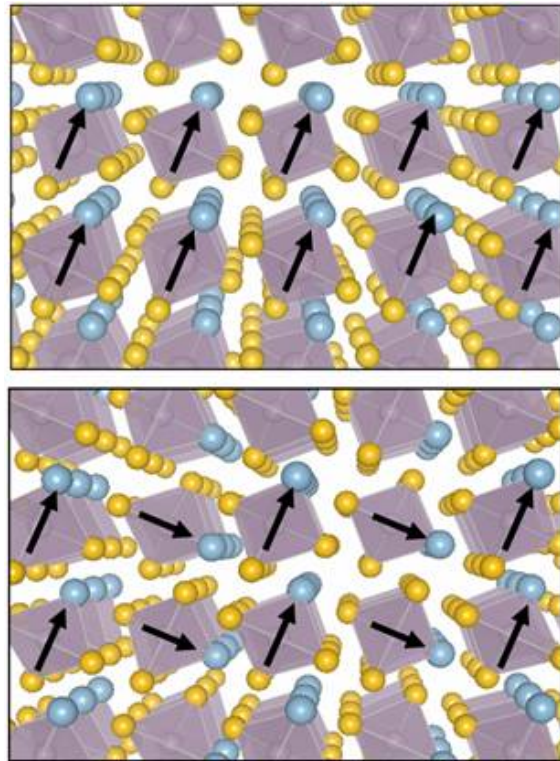


**Figure 24:** Polyhedral representation of the Si<sub>3</sub>AlP crystal structure corresponding to two distinct arrangements of the AlPSi<sub>3</sub> units. The black arrows indicate the direction of the P-Al bonds.

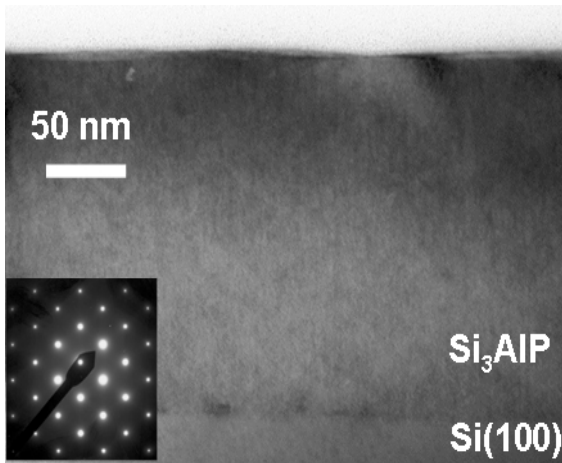
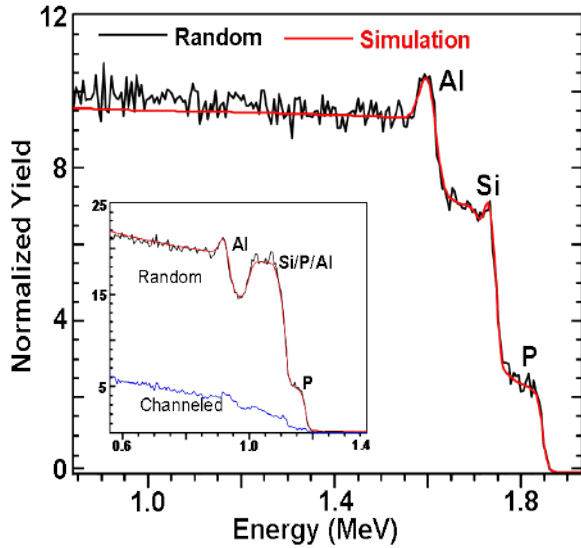


**Figure 25:** Representative RBS spectra of Si/P/Al films. (Top) 3 MeV spectrum showing well separated P, Si and Al signals. Fits to these data and those from a 2 MeV analogs yield an average composition of  $\text{Al}_{0.9}\text{PSi}_{2.95}$  and a thickness of 190 nm. (Inset) 2 MeV spectrum of an  $\text{AlPSi}_{2.90}$  film with 400 nm thickness showing a significant overlap of the RBS peaks and a remarkably high degree of channeling. (Bottom) XTEM micro graph and diffraction pattern of the 190 nm thick sample showing a defect free layer perfectly lattice matched to Si.

on (III-V)-(IV) materials has been on the wane for the past 10 years. Very recently, however, we have introduced an entirely new approach to the synthesis of (III-V)-(IV) materials that is specifically designed to avoid phase separation. As an initial proof of concept, we demonstrated the growth of  $\text{Si}_3\text{AlP}$  on Si (100) substrates.<sup>49</sup> Key to this success is the use of the  $(\text{H}_3\text{Si})_3\text{P}$  molecule as a growth precursor. When  $(\text{H}_3\text{Si})_3\text{P}$  combines with Al atoms generated from a Knudsen cell, it is envisioned to form “Al:P( $\text{SiH}_3$ )<sub>3</sub>” intermediate complexes from which the (Al-P)- $\text{Si}_3$  tetrahedron can be incorporated intact into the growing diamond-like solid (see Fig. 24) by elimination of the terminal Si-H bonds under low temperature ( $\sim 500^\circ\text{C}$ ) conditions.<sup>49</sup> The  $(\text{IV})_3(\text{III-V})$  formula is unique to our approach and corresponds to the lowest group-IV concentration for which the III-V elements can be accommodated in the lattice as *isolated* “donor-acceptor” pairs. Such configurations prevent phase segregation and defects, leading to materials with high crystallinity which grow perfectly lattice matched on Si substrates, as seen in Fig. 25. We subsequently extended the concept to the demonstration of alloys of the form  $\text{Si}_{5-2x}(\text{AlP})_x$  spanning the whole range of concentrations between pure Si and stoichiometric  $\text{Si}_3\text{AlP}$ . Most recently, we have synthesized  $\text{Si}_3\text{AlAs}$ ,  $\text{Si}_3\text{Al}(\text{As}_{1-x}\text{P}_x)$ , and  $\text{Si}_3\text{Al}(\text{As}_{1-x}\text{N}_x)$ , demonstrating that the process can be generalized to systems in which the III-V and IV-IV natural bond lengths are dissimilar.

## Personnel

The MURI program made a substantial contribution to the formation of human resources. Eight students received PhDs with support from the MURI program, and 2 postdocs were also supported.

**ASU:** Students Vijay R. D'Costa, Yan Yan Fang, Junqi Xie, Chang'e Weng, Jesse Tice, Yu Jing, and Jay Mathews received full or partial support from the MURI grant and successfully defended their PhD dissertation during this period. Student Brandon Forrrest received a Masters degree in Chemistry. The program also supported post-docs Dr. Radek Roucka and Dr. Vijay D'Costa.

**U. of Illinois:** Students Shu-Wei Chang and Chi-Yu Ni received full or partial support from the MURI grant, in addition to visiting scholar Dr. Guoen Chang.

**U. Mass:** The program provided partial support for co-PI Greg Sun, Research Associate Fenyen Chang, and graduate student Can Lu.

## Grant Refereed Publications

- 1 V. R. D'Costa, J. Tolle, C. D. Poweleit, J. Kouvetakis, and J. Menéndez, *Phys. Rev. B* 76 (3), 035211 (2007).
- 2 J. Tolle, A. V. G. Chizmeshya, Y. Y. Fang, J. Kouvetakis, V. R. D'Costa, C. W. Hu, J. Menéndez, and I. S. T. Tsong, *Appl. Phys. Lett.* 89 (23), 231924 (2006).
- 3 J. B. Tice, A. V. G. Chizmeshya, R. Roucka, J. Tolle, B. R. Cherry, and J. Kouvetakis, *J. Am. Chem. Soc.* 129 (25), 7950 (2007).
- 4 G. Sun, H. H. Cheng, J. Menendez, J. B. Khurgin, and R. A. Soref, *Appl. Phys. Lett.* 90 (25), 251105 (2007).
- 5 S.-W. Chang and S. L. Chuang, *IEEE J. Quant. Electron.* 43 (3), 249 (2007).
- 6 M. A. Wistey, Y. Y. Fang, J. Tolle, A. V. G. Chizmeshya, and J. Kouvetakis, *Appl. Phys. Lett.* 90 (8), 082108 (2007).
- 7 Y. Y. Fang, J. Tolle, R. Roucka, A. V. G. Chizmeshya, J. Kouvetakis, V. R. D'Costa, and J. Menendez, *Appl. Phys. Lett.* 90 (6), 061915 (2007).
- 8 J. Kouvetakis and A. V. G. Chizmeshya, *Journal of Materials Chemistry* 17 (17), 1649 (2007).
- 9 R. A. Soref, J. Kouvetakis, J. Menéndez, J. Tolle, and V. R. D'Costa, *Journal of Materials Research* 22 (12), 3281 (2007).
- 10 V. R. D'Costa, J. Tolle, R. Roucka, C. D. Poweleit, J. Kouvetakis, and J. Menendez, *Solid State Commun.* 144 (5-6), 240 (2007).
- 11 Y.-Y. Fang, J. Tolle, J. Tice, A. V. G. Chizmeshya, J. Kouvetakis, V. R. D'Costa, and J. Menéndez, *Chemistry of Materials* 19 (24), 5910 (2007).
- 12 K. M. Hung, T. H. Cheng, W. P. Huang, K. Y. Wang, H. H. Cheng, G. Sun, and R. A. Soref, *Appl. Phys. Lett.* 93 (12), 123509 (2008).
- 13 J. B. Tice, Y. Y. Fang, J. Tolle, A. Chizmeshya, and J. Kouvetakis, *Chemistry of Materials* 20 (13 %R doi:10.1021/cm800427p), 4374 (2008).
- 14 J. Kouvetakis, Y. J. An, V. R. D'Costa, J. Tolle, A. V. G. Chizmeshya, and J. Menéndez, *J. Mater. Chem.* 18, 4775 (2008).
- 15 J. Kouvetakis, J. Tolle, R. Roucka, V. R. D'Costa, Y.-Y. Fang, A. V. Chizmeshya, and J. Menendez, *ECS Transactions* 16 (10), 807 (2008).
- 16 Y. Y. Fang, V. R. D'Costa, J. Tolle, C. D. Poweleit, J. Kouvetakis, and J. Menéndez, *Thin Solid Films* 516 (23), 8327 (2008).

- 17 Y.-Y. Fang, J. Xie, J. Tolle, R. Roucka, V. R. D'Costa, A. V. G. Chizmeshya, J. Menendez, and J. Kouvetakis, *J. Am. Chem. Soc.* 130 (47), 16095 (2008).
- 18 R. Roucka, J. Xie, J. Kouvetakis, J. Mathews, V. D. Costa, J. Menendez, J. Tolle, and S. Q. Yu, *J. Vac. Sci. Technol. B* 26 (6), 1952 (2008).
- 19 R. Roucka, Y. J. An, A. V. G. Chizmeshya, V. R. D'Costa, J. Tolle, J. Menéndez, and J. Kouvetakis, *Solid-State Electronics* 52 (11), 1687 (2008).
- 20 Y. Y. Fang, V. R. D'Costa, J. Tolle, J. B. Tice, C. D. Poweleit, J. Menéndez, and J. Kouvetakis, *Solid State Commun.* 149 (1-2), 78 (2009).
- 21 J. Q. Xie, J. Tolle, V. R. D'Costa, C. Weng, A. V. G. Chizmeshya, J. Menendez, and J. Kouvetakis, *Solid-State Electronics* 53 (8), 816 (2009).
- 22 J. Menéndez, *J. Appl. Phys.* 105 (6), 063519 (2009).
- 23 V. R. D'Costa, Y. Y. Fang, J. Tolle, J. Kouvetakis, and J. Menendez, *Phys. Rev. Lett.* 102 (10), 107403 (2009).
- 24 Y. Y. Fang, J. Tolle, A. V. G. Chizmeshya, J. Kouvetakis, V. R. D'Costa, and J. Menendez, *Appl. Phys. Lett.* 95 (8), 081113 (2009).
- 25 G.-E. Chang, S.-W. Chang, and S. L. Chuang, *Opt. Express* 17 (14), 11246 (2009).
- 26 J. B. Tice, C. G. Weng, J. Tolle, V. R. D'Costa, R. Singh, J. Menendez, J. Kouvetakis, and A. V. G. Chizmeshya, *Dalton Transactions* (34), 6773 (2009).
- 27 J. Tolle, R. Roucka, B. Forrest, A. V. G. Chizmeshya, J. Kouvetakis, V. R. D'Costa, C. D. Poweleit, M. Groenert, T. Sato, and J. Menendez, *Chemistry Of Materials* 21 (14), 3143 (2009).
- 28 V. R. D'Costa, J. Tolle, J. Q. Xie, J. Kouvetakis, and J. Menendez, *Phys. Rev. B* 80 (12), 125209 (2009).
- 29 J. Mathews, R. Roucka, J. Q. Xie, S. Q. Yu, J. Menendez, and J. Kouvetakis, *Appl. Phys. Lett.* 95 (13), 133506 (2009).
- 30 V. R. D'Costa, Y. Fang, J. Mathews, R. Roucka, J. Tolle, J. Menendez, and J. Kouvetakis, *Semicond. Sci. Technol.* 24 (11), 115006 (2009).
- 31 J. Xie, J. Tolle, V. R. D'Costa, A. V. G. Chizmeshya, J. Menéndez, and J. Kouvetakis, *Appl. Phys. Lett.* 95 (18), 181909 (2009).
- 32 J. B. Tice, A. V. Chizmeshya, T. L. Groy, and J. Kouvetakis, *Inorg Chem* 48 (13), 6314 (2009).
- 33 V. R. D'Costa, Y. Y. Fang, J. Tolle, J. Kouvetakis, and J. Menéndez, *Thin Solid Films* 518 (9), 2531 (2010).

- 34 A. V. Chizmeshya and J. Kouvetakis, *ECS Transactions* 33 (6), 717 (2010).
- 35 J. Kouvetakis, J. Mathews, R. Roucka, A. V. G. Chizmeshya, J. Tolle, and J. Menendez, *IEEE Photonics J.* 2 (6), 924 (2010).
- 36 J. Kouvetakis, J. Tolle, J. Mathews, R. Roucka, and J. Menendez, *ECS Transactions* 33 (6), 615 (2010).
- 37 J. Mathews, R. T. Beeler, J. Tolle, C. Xu, R. Roucka, J. Kouvetakis, and J. Menéndez, *Appl. Phys. Lett.* 97 (22), 221912 (2010).
- 38 R. Roucka, Y. Y. Fang, J. Kouvetakis, A. V. G. Chizmeshya, and J. Menéndez, *Phys. Rev. B* 81 (24), 245214 (2010).
- 39 J. B. Tice, A. V. G. Chizmeshya, J. Tolle, V. R. D'Costa, J. Menendez, and J. Kouvetakis, *Dalton Transactions* 39 (19), 4551 (2010).
- 40 J. B. Tice, V. R. D'Costa, G. Grzybowski, A. V. G. Chizmeshya, J. Tolle, J. Menendez, and J. Kouvetakis, *Chemistry of Materials* 22 (18), 5296 (2010).
- 41 C. Weng, J. Kouvetakis, and A. V. G. Chizmeshya, *Chemistry of Materials* 22, 3884 (2010).
- 42 J. Xie, A. V. G. Chizmeshya, J. Tolle, V. R. D'Costa, J. Menendez, and J. Kouvetakis, *Chemistry of Materials* 22 (12), 3779 (2010).
- 43 G. Sun, R. A. Soref, and H. H. Cheng, *J. Appl. Phys.* 108 (3), 033107 (2010).
- 44 G. Sun, R. A. Soref, and H. H. Cheng, *Opt. Express* 18 (19), 19957 (2010).
- 45 R. Beeler, R. Roucka, A. Chizmeshya, J. Kouvetakis, and J. Menéndez, *Phys. Rev. B* 84 (3) (2011).
- 46 R. T. Beeler, G. J. Grzybowski, R. Roucka, L. Jiang, J. Mathews, D. J. Smith, J. Menéndez, A. V. G. Chizmeshya, and J. Kouvetakis, *Chemistry of Materials* 23 (20), 4480 (2011).
- 47 G. Grzybowski, L. Jiang, J. Mathews, R. Roucka, C. Xu, R. T. Beeler, J. Kouvetakis, and J. Menéndez, *Appl. Phys. Lett.* 99 (17), 171910 (2011).
- 48 G. Grzybowski, R. Roucka, J. Mathews, L. Jiang, R. Beeler, J. Kouvetakis, and J. Menéndez, *Phys. Rev. B* 84 (20) (2011).
- 49 T. Watkins, A. V. Chizmeshya, L. Jiang, D. J. Smith, R. T. Beeler, G. Grzybowski, C. D. Poweleit, J. Menendez, and J. Kouvetakis, *J. Am. Chem. Soc.* 133 (40), 16212 (2011).
- 50 S. Bagchi, C. Poweleit, R. Beeler, J. Kouvetakis, and J. Menéndez, *Phys. Rev. B* 84 (19) (2011).

<sup>51</sup> G.-E. Chang, S.-W. Chang, and S. L. Chuang, Quantum Electronics, IEEE Journal of 46 (12), 1813 (2010).

## References

- <sup>52</sup> M. Bauer, C. Ritter, P. A. Crozier, J. Ren, J. Menéndez, G. Wolf, and J. Kouvetakis, *Appl. Phys. Lett.* 83 (11), 2163 (2003).
- <sup>53</sup> J. Tolle, R. Roucka, A. V. G. Chizmeshya, J. Kouvetakis, V. R. D'Costa, and J. Menendez, *Appl. Phys. Lett.* 88 (25), 252112 (2006).
- <sup>54</sup> V. R. D'Costa, C. S. Cook, A. G. Birdwell, C. L. Littler, M. Canonico, S. Zollner, J. Kouvetakis, and J. Menendez, *Phys. Rev. B* 73 (12), 125207 (2006).
- <sup>55</sup> V. R. D'Costa, C. S. Cook, J. Menendez, J. Tolle, J. Kouvetakis, and S. Zollner, *Solid State Commun.* 138 (6), 309 (2006).
- <sup>56</sup> R. Roucka, R. Beeler, J. Mathews, M.-Y. Ryu, Y. Kee Yeo, J. Menéndez, and J. Kouvetakis, *J. Appl. Phys.* 109 (10), 103115 (2011).
- <sup>57</sup> R. Roucka, J. Mathews, C. Weng, R. Beeler, J. Tolle, J. Menendez, and J. Kouvetakis, *IEEE J. Quant. Electron.* 47 (2), 213 (2011).
- <sup>58</sup> R. Roucka, J. Mathews, R. T. Beeler, J. Tolle, J. Kouvetakis, and J. Menéndez, *Appl. Phys. Lett.* 98 (6), 061109 (2011).
- <sup>59</sup> S. Yerci, R. Li, S. O. Kucheyev, T. v. Buuren, S. N. Basu, and L. D. Negro, *Appl. Phys. Lett.* 95 (3), 031107 (2009).
- <sup>60</sup> A. J. Noreika and M. H. Francombe, *J. Appl. Phys.* 45 (8), 3690 (1974).
- <sup>61</sup> K. C. Cadien, A. H. Eltoukhy, and J. E. Greene, *Appl. Phys. Lett.* 38 (10), 773 (1981).
- <sup>62</sup> I. Banerjee, D. W. Chung, and H. Kroemer, *Appl. Phys. Lett.* 46 (5), 494 (1985).
- <sup>63</sup> A. G. Norman, J. M. Olson, J. F. Geisz, H. R. Moutinho, A. Mason, M. M. Al-Jassim, and S. M. Vernon, *Appl. Phys. Lett.* 74 (10), 1382 (1999).
- <sup>64</sup> K. Newman and J. Dow, *Phys. Rev. B* 27 (12), 7495 (1983).
- <sup>65</sup> J. Greene, *J. Vac. Sci. Technol. B* 1 (2), 229 (1983).
- <sup>66</sup> V. L. Solozhenko, D. Andrault, G. Fiquet, M. Mezouar, and D. C. Rubie, *Appl. Phys. Lett.* 78 (10), 1385 (2001).
- <sup>67</sup> T. C. McGlinn, M. V. Klein, L. T. Romano, and J. E. Greene, *Phys. Rev. B* 38 (5), 3362 (1988).